International Journal of Nanomedicine Dovepress

Open Access Full Text Article ORIGINAL RESEARCH

A Multifunctional Nanodrug Co-Delivering VEGF-siRNA and Dexamethasone for Synergistic Therapy in Ocular Neovascular Diseases

Xiaochen Ma[1], Yubo Cui[2], Min Zhang[1], Qinghua Lyu[2], Jun Zhao[2]

[1]The Second Clinical Medical College, Jinan University, Shenzhen, Guangdong, People's Republic of China; [2]Department of Ophthalmology, Shenzhen People's Hospital (The Second Clinical Medical College, Jinan University; The First Affiliated Hospital, Southern University of Science and Technology), Shenzhen, Guangdong, People's Republic of China

Correspondence: Qinghua Lyu; Jun Zhao, Department of Ophthalmology, Shenzhen People's Hospital (The Second Clinical Medical College, Jinan University; The First Affiliated Hospital, Southern University of Science and Technology), Shenzhen, 518020, People's Republic of China, Email a0129473@u.nus.edu; doctorzhaojun@163.com

Introduction: Oxidant stress, abnormal angiogenesis, and inflammation are three key factors contributing to the development of ocular neovascular diseases (ONDs). This study aims to develop a multifunctional nanodrug, DEX@MPDA-Arg@Si (DMAS), which integrates mesoporous polydopamine, vascular endothelial growth factor (VEGF)-siRNA, and dexamethasone (DEX) to address these therapeutic targets.

Methods: Physicochemical properties of DMAS were measured using transmission electron microscopy and a nanoparticle size analyzer. The encapsulation efficiency and drug loading capacity of DMAS were measured using a UV-visible spectrophotometer. The in vivo therapeutic efficacy and ocular safety of DMAS were evaluated using three established mouse models, including the alkali burn-induced corneal neovascularization (CoNV) model, the oxygen-induced retinopathy (OIR) model, and the laser-induced choroidal neovascularization (CNV) model.

Results: The DMAS nanoparticles demonstrated a uniform bowl-like shape with an average size of 264.9 ± 2.5 nm and a zeta potential of −28.2 ± 4.2 mV. They exhibited high drug-loading efficiency (36.04 ± 3.60% for DEX) and excellent biocompatibility. In vitro studies confirmed its potent antioxidant, anti-inflammatory, and anti-apoptotic properties. In vivo, DMAS treatment led to significant therapeutic effects across all models. It effectively inhibited CoNV, promoted corneal repair, and modulated inflammation in the alkali burn model. In the OIR model, DMAS reduced retinal neovascularization by decreasing VEGF expression. In the laser-induced CNV model, it significantly reduced the CNV area and lesion thickness.

Conclusion: This research developed a multifunctional nanodrug, DMAS, capable of co-delivering VEGF-siRNA and DEX, offering synergistic therapeutic benefits for treating ONDs. The DMAS nanodrug demonstrates promising anti-inflammatory, antioxidative, and anti-angiogenic effects, highlighting its potential as a versatile and effective treatment for multiple ocular conditions.

Keywords: mesoporous polydopamine, nano-delivery platform, ocular neovascular diseases, dexamethasone, VEGF-siRNA

Introduction

Ocular neovascular diseases (ONDs) are a major focus in ophthalmic research due to their prevalence and significant impact on vision.[1,2] The pathological process of ONDs involves abnormal angiogenesis in the cornea, retina, and choroid, leading to conditions such as corneal neovascularization (CoNV), retinopathy of prematurity (ROP), diabetic retinopathy (DR), and neovascular age-related macular degeneration (nAMD).[3] The core issue in ONDs is the dysregulated expression of vascular endothelial growth factor (VEGF), a crucial pro-angiogenic cytokine that promotes endothelial cell proliferation and new vessel formation.[4] This dysregulation is often intensified by inflammatory mediators like tumor necrosis factor-alpha (TNF-α), interleukin-6 (IL-6), and interleukin-1 beta (IL-1β), which collectively enhance VEGF activity and angiogenic pathways.[5] Additionally, reactive oxygen species (ROS) and oxidative stress further drive neovascularization by upregulating VEGF and activating signaling pathways, particularly in nAMD.[6] Due to these complex mechanisms, effective clinical management

Received: 22 August 2024
Accepted: 13 November 2024
Published: 21 November 2024

requires a comprehensive therapeutic strategy, combining anti-VEGF agents, anti-inflammatory treatments, and antioxidants to control disease progression and preserve vision.

Currently, two main therapeutic approaches are utilized for treating ONDs: anti-VEGF agents, such as aflibercept and bevacizumab, and corticosteroids.[7,8] Anti-VEGF therapies, primarily formulated as fusion proteins or antibodies, function by binding to and neutralizing VEGF, which effectively inhibits angiogenic signaling pathways and reduces neovascularization.[9,10] In addition to anti-VEGF agents, corticosteroids are widely used due to their ability to alleviate inflammation, inhibit the proliferation of capillaries and leukocytes, reduce edema, and suppress disease progression in ocular neovascular conditions.[11–14] For example, Goswami et al found that dexamethasone (DEX) modulated inflammation and neovascularization through VEGF pathways.[15] Kadar et al emphasized that early anti-inflammatory treatments, including steroids and VEGF inhibitors like bevacizumab, significantly reduced corneal neovascularization and inflammation in chemically-induced ocular injuries.[8] Together, these findings underscore the therapeutic advantages of combining DEX and VEGF inhibition for ONDs. Despite the promising results of both VEGF inhibitors and corticosteroids, regardless of whether administered alone or together,[16] these therapies often require repeated doses, which can lead to increased treatment complexity, elevated costs, and heightened risks of adverse effects.[17]

In addition to the costly VEGF-antibody used for various diseases, small interfering RNA (siRNA) technology has garnered significant attention in recent years due to its affordability and accessibility for treating VEGF-related diseases.[18,19] Currently, VEGF-siRNA therapies, such as ALN-VSP developed by Alnylam Pharmaceuticals,[20,21] are primarily intended for cancer treatment, with few applications in ophthalmic diseases such as Bevasiranib for nAMD.[22] Despite these advances, the clinical translation of siRNA molecules faces significant challenges, particularly in the precise delivery and inhibition of off-target effects such as the activation of Toll-like receptors.[23–25] To enhance the delivery efficiency and targeting specificity of siRNA, a variety of nanomaterials, including lipid nanoparticles (NPs) and bioactive NPs such as polydopamine (PDA), have been developed.[26–29] Moreover, these nanomaterials not only address issues such as degradation and low permeability of siRNA, but they also expand its application to a wide range of diseases.[30–33]

To address the clinical need for treating ONDs, we developed a multifunctional nanodrug, DEX@MPDA-Arg@Si (DMAS), by integrating bioactive mesoporous polydopamine (MPDA) with VEGF-siRNA and DEX. The multifunctional nanocarrier MPDA was selected to load the two agents primarily due to its larger specific surface area, richer pore structure, more active binding sites, and excellent biocompatibility as compared to lipidic and polymeric nanoparticles.[34,35] In addition to its physical advantages, the melanin-mimicking MPDA, by virtue of its multifaceted biological properties—including anti-inflammatory, anti-ROS, tissue regeneration promotion, anti-angiogenesis, and immunomodulation—renders itself as a promising nanocarrier for treating various diseases.[31,36–38]

Nanodrug co-delivery systems enhance therapeutic efficacy by combining drugs that target different aspects of a disease, thereby producing synergistic effects.[39,40] In clinical cases, the combination of a DEX implant with bevacizumab has been demonstrated to significantly improve visual acuity and macular morphology in eyes with refractory diabetic macular edema.[41] The nanodrug DMAS was designed to provide synergistic therapeutic effects through VEGF-siRNA, DEX, and MPDA, aiming to reduce treatment frequency and duration, lower costs, mitigate side effects, and improve patient outcomes. To test this, we selected three established animal models—CoNV, oxygen-induced retinopathy (OIR), and laser-induced choroidal neovascularization (CNV)—representing neovascular diseases in the cornea, retina, and choroid. To our knowledge, this study is the first to explore an integrated delivery system combining gene therapy, corticosteroids, and bioactive MPDA for OND treatment.

Materials and Methods

Preparation and Characterization of MPDA Nanodrugs

Following a published method,[42] MPDA was synthesized by dissolving 150 mg of dopamine hydrochloride (Cat# D103111, Aladdin, Shanghai, China) in 3 mL deionized water and 100 mg of Pluronic F127 (Cat# P6790, Solarbio, Beijing, China) in 3 mL ethanol. After combining these solutions, 160 μL of 1,3,5-trimethylbenzene (Cat# T818958, Macklin, Shanghai, China) and 375 μL of 28% NH_4OH were added, followed by stirring with 1 mL of L-arginine solution (150 mg/mL) (Cat# HY-N0455, MedChemExpress, Monmouth Junction, NJ, USA) in the dark for 6 hours.[43]

The resulting MPDA-Arg (MA) nanoparticles were washed and subsequently loaded with DEX (Cat# HY-14648, MedChemExpress, Monmouth Junction, NJ, USA) to form DEX@MPDA-Arg (DMA). For siRNA loading, DMA at various concentrations was mixed with 50 nM siRNA to create DEX@MPDA-Arg@Si (DMAS). The detailed procedures are presented in the Supplementary Materials section. The nanoparticle morphology of MPDA nanodrugs (including MA, DMA, and DMAS) was examined using a G2 F30 S-Twin transmission electron microscope (TEM) (Tecnai, Oregon, USA). Zeta potentials and particle sizes were measured with a Malvern Zetasizer Nano instrument (Malvern, Worcestershire, UK).

Cytocompatibility of MPDA Nanodrugs

Human umbilical vein endothelial cell (HUVEC) and RAW264.7 cells (BIOSPECIES, Guangzhou, China) (5×10^3 cells per well) were seeded onto 96-well plates and incubated at 37°C for 24 hours, serving as in vitro model systems for vascular and inflammatory studies, respectively. Subsequently, the cells were exposed to varying concentrations (5–150 μg/mL) of nanodrugs for an additional 24 hours. Then, the original medium was aspirated and replaced with fresh complete medium. The cells were then incubated with CCK-8 solution for 2 hours. Cytotoxicity of the MPDA nanodrugs was assessed using the CCK-8 assay (Biosharp, Hefei, China).

Intracellular ROS-Scavenging Ability of MPDA Nanodrugs

RAW264.7 cells (3×10^5 cells per well) were cultured with MPDA nanodrugs on cell slides in a 24-well plate for 24 hours. ROS was induced by adding hydrogen peroxide (H_2O_2) (100 μM) to each well for 2 hours. RAW264.7 cells were stained with 2',7'-dichlorodihydrofluorescein diacetate (DCFH-DA, Biosharp, Hefei, China) (10 μM) for another 1 hour. Finally, the cells were imaged using a DMi8 fluorescence microscope (Leica, Hamburg, Germany). Quantitative analysis of the average fluorescence intensity was performed with ImageJ software.

Effects of MPDA Nanodrugs on Cellular Cytokines and VEGF Expression

HUVEC and RAW264.7 cells (2×10^5 cells per well) were individually exposed to 1 μg/mL lipopolysaccharide (LPS, Cat# L970739, Macklin, Shanghai, China) in a 24-well plate for 2 hours, followed by treatment with various nanodrugs for 24 hours. Subsequently, the cell supernatant was collected and centrifuged for enzyme-linked immunosorbent assay analysis to determine the concentrations of TNF-α, IL-6, IL-1β, and VEGF (Solarbio, Beijing, China) using a microplate reader (BioTek, Winooski, USA).

Effects of MPDA Nanodrugs on Cell Apoptosis

HUVEC and RAW264.7 cells were individually exposed to 1 μg/mL LPS for 2 hours. Following treatment with MPDA nanodrugs for 24 hours, the cells (1×10^6 cells per well) were collected, rinsed with phosphate-buffered saline (PBS), and suspended in 400 μL of binding buffer. Annexin V-FITC and PI (Solarbio, Beijing, China) were then added and incubated in the dark for 15 minutes. Finally, flow cytometry analysis was promptly conducted within 30 minutes using the DxFLEX flow cytometer (Beckman, CA, USA).

Establishment of Three Ocular Neovascular Animal Models

Three ocular neovascular models, including alkali burn-induced CoNV mouse model, OIR mouse model, and laser-induced CNV mouse model, were established by following several reported methods. The experimental details are provided in the Supplementary Materials section. Female BALB/c and C57BL/6J mice (6−8 weeks old) were sourced from Vital River Experimental Animals Technology (Beijing, China). This study and the included experimental procedures were approved by the Institutional Animal Care and Use Committee of Shenzhen People's Hospital (License No. LL-KY-2021541). All animal housing and experiments were conducted in strict accordance with the institutional guidelines for the care and use of laboratory animals.

Ocular Injections of MPDA Nanodrugs

The mice were sedated with 2% isoflurane via a disposable mask using a small animal anesthesia machine (RWD, Shenzhen, China). The formulations (1 mg/mL of MA, DMA, or DMAS and 5 mg/mL of DEX) were prepared for all injection methods. For subconjunctival injection in the CoNV model, 5 μL of the prepared formulation was injected into the temporal subconjunctival zone using a Hamilton microsyringe (Hamilton, Nevada, USA). Intravitreal injections were administered via a scleral incision 1 mm posterior to the limbus, delivering the formulations into the vitreous chamber using a Hamilton syringe. In the OIR mouse model, the administered drug volume was 1 μL, while in the laser-induced CNV mouse model, the volume was increased to 1.5 μL. The drugs were administered on days 1, 4, 7, and 10 post-modeling. For the OIR model, treatment started when the mice were returned to room air.

Ophthalmic Examination on Corneal Neovascularization Mouse Model

For corneal fluorescein staining, 1 μL of 2% fluorescein sodium (Aladdin, Shanghai, China) solution was administered into the conjunctival sac for 10 seconds. Subsequently, the eye was flushed with PBS to eliminate excess fluorescein sodium. The defects in the corneal epithelium were promptly examined under cobalt blue light using a slit lamp biomicroscope (Carl Zeiss, Oberkochen, Germany). Corneal optical opacity was graded on a scale of 0 to 4, referencing the standard images (Supplementary Figure S1). Evaluation of CoNV was conducted using a modified scoring system.[44,45] Each of the five corneal regions (inferior, superior, temporal, nasal, and central) received a score from 0 to 4 depending on neovascularization coverage: 0 for no vessels, 1 for less than 30%, 2 for 30–70%, 3 for 70–100%, and 4 for full coverage. When measuring the CoNV length, the longest CoNV with good continuity and minimal curvature was selected. Optical coherence tomography (OCT) images of the anterior segment and fundus were captured using the CIRRUS HD-OCT 5000 device (Carl Zeiss, Oberkochen, Germany). Corneal thickness and anterior chamber depth were calculated by the OCT built-in software.

Ophthalmic Examination on Fundus Neovascularization Mouse Model

Following anesthesia, a drop of tropicamide (Santen, Osaka, Japan) was instilled into both eyes of the mice to achieve pupil dilation for in vivo fundus color imaging and vascular fluorescence angiography. Subsequently, Hylo-Comod eye drops (Ursapharm, Saarbrücken, Germany) were administered to maintain ocular surface moisture. After white balance calibration, the fundus color photography was captured and saved using the Phoenix Micron IV fundus imaging system (Phoenix, Oregon, USA). Subsequently, the mice received an intraperitoneal injection of 0.1 mL of 2.5% sodium fluorescein (Macklin, Shanghai, China). After 3 minutes, when the sodium fluorescein had sufficiently entered the bloodstream, images of the fundus fluorescein angiography were captured and saved in fluorescein photography mode (Phoenix, Oregon, USA).

Flow Cytometry Analysis in Conjunctival Tissue

Mouse conjunctival tissue was separated and then digested in Dulbecco's Modified Eagle Medium supplemented with 2 mg/mL collagenase (ACMEC, Shanghai, China) and 5 mg/mL DNase (Solarbio, Beijing, China) for 2 hours at 37 °C. The conjunctival tissue suspension was filtered through a 70-μm cell strainer (BD, Franklin Lakes, NJ, USA). Single cells in suspension were then immunostained with anti-mouse F4/80 antibody (Cat# 157303, PE-conjugated, diluted at 1:100, BioLegend, San Diego, CA, USA) and anti-mouse CD31 antibody (Cat# 102405, FITC-conjugated, diluted at 1:100, BioLegend, San Diego, CA, USA). Flow cytometric analysis of the stained cells was conducted using the DxFLEX flow cytometer (Beckman, Brea, CA, USA) and FCS Express software.

Retina and RPE/Choroid Flat-Mount Immunofluorescent Staining with IB4

Retina and choroid were separated after the removal of cornea, lens, and vitreous from the eye. The retinas and retinal pigment epithelium (RPE)/choroid were permeabilized in PBS containing 0.3% Triton X-100 (Sangon Biotech, Shanghai, China) at 4°C for 4 hours, and blocked with 0.5% bovine serum albumin (Servicebio, Beijing, China) at 4°C for 6 hours. After three washes with PBS, the retinal samples and RPE/choroid were incubated with fluorescein-conjugated isolectin B4 (IB4, Cat#

FL-1201, diluted at 1:100, Vector Laboratories, Burlingame, USA) at 4°C overnight. Finally, the samples were divided into four quadrants by four radial incisions and mounted on a slide with a coverslip. The immunofluorescent images of the retinal vasculature and CNV were captured by a DMi8 digital fluorescence microscope. The areas of retinal neovascularization, non-perfused retinal regions, and CNV were measured using ImageJ software.[46]

Statistical Analysis

Statistical analyses were performed using GraphPad Prism software (version 9.5.0). Group comparisons were assessed using an unpaired, two-tailed Student's *t*-test for two-group comparisons, while one-way ANOVA with Tukey's post hoc test was used for comparisons involving more than two groups. A value of $P < 0.05$ was considered statistically significant.

Results

Synthesis and Characterization of MPDA Nanodrugs

The synthesis of DMAS is illustrated in Figure 1, which highlights two primary stages: the fabrication of MPDA NPs and the subsequent incorporation of DEX and VEGF-siRNA onto MPDA NPs. A previously reported VEGF-siRNA was used in our experiment,[47] with the specific sequences provided in Supplementary Materials Table 1.

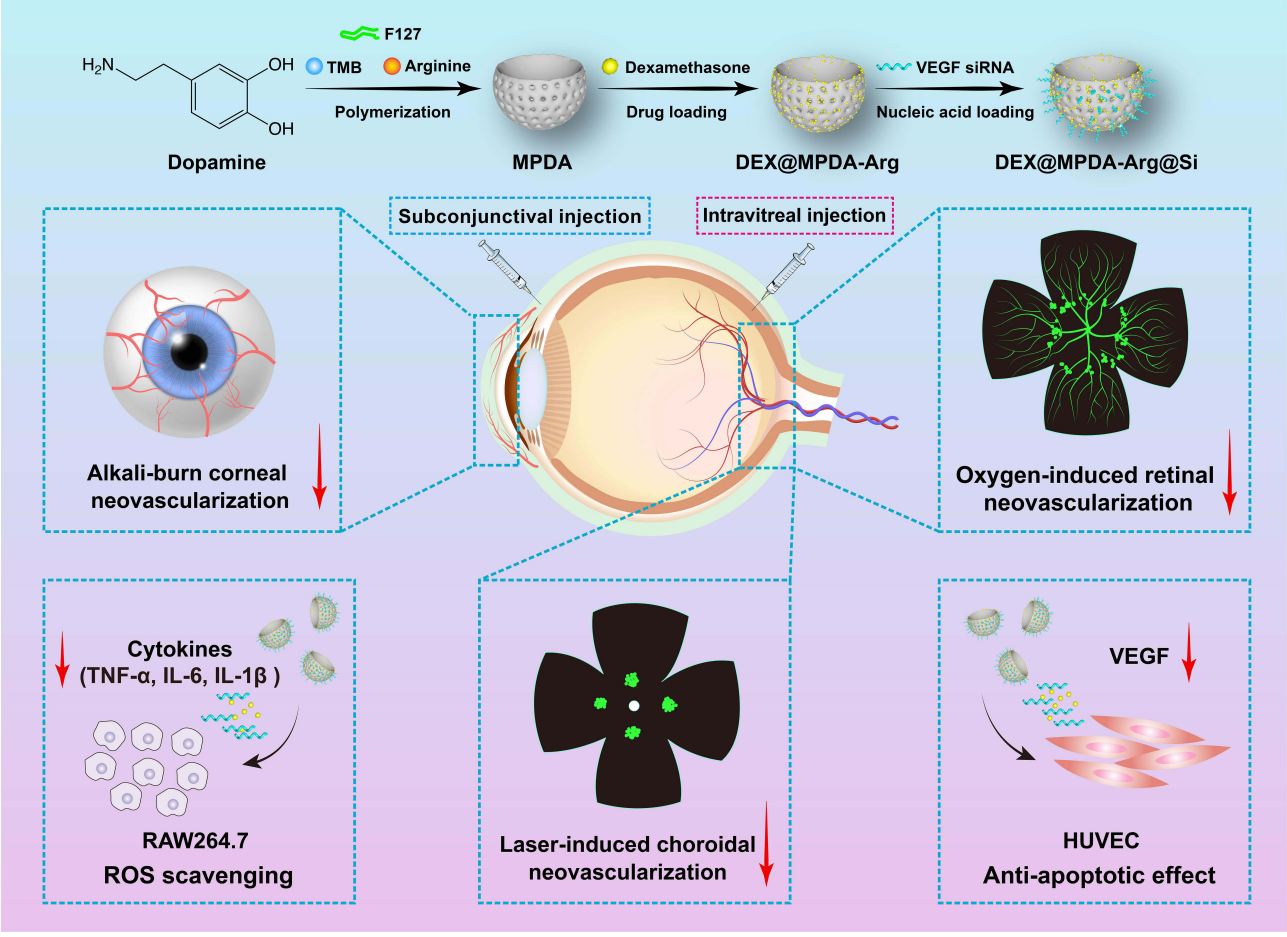

Figure 1 A schematic diagram of DMAS nanodrug for ONDs. This picture depicts the preparation of MPDA nanodrugs, including polymerization and drug loading processes, as well as their therapeutic effects in various OND models, such as the alkali burn-induced CoNV model, OIR model, and laser-induced CNV model. Through subconjunctival and intravitreal injections, MPDA nanodrugs exhibit multiple therapeutic effects. At the animal level, they effectively reduce neovascularization. At the cellular level, they inhibit the expression of inflammatory cytokines (such as TNF-α, IL-6, and IL-1β) and possess ROS-scavenging capability.

The physicochemical properties of the MPDA nanodrugs were characterized, mainly focusing on their morphological structure, size, surface potential, and stability. Macroscopic observations revealed that high concentrations of MPDA nanodrugs displayed a brownish-black color (Supplementary Figure S2A). TEM analysis confirmed that DMAS nanodrugs exhibited a typical bowl-like morphology, with uniformly distributed mesoporous structures on their surface and a consistent size distribution (Supplementary Figure S2B). The mesoporous structure of PDA provides a high surface area, which facilitates adsorption and encapsulation of therapeutic agents such as DEX and siRNA. The zeta potential of DMAS was approximately −28.2 ± 4.2 mV (Supplementary Figure S2C), close to the optimal zeta potential of −30 mV as reported previously.[48] The average particle size of MA was approximately 262.5 ± 1.9 nm (Supplementary Figure S2D). After loading with DEX and siRNA, the particle size of DMAS slightly increased to 264.9 ± 2.5 nm (Supplementary Figure S2E), indicating that the incorporation of small molecule drugs into the pores of MPDA nanodrugs did not significantly change the particle size. The particle size of these MPDA nanodrugs is consistent with other reports ranging from 100 to 300 nm.[35,49,50] A two-week experiment monitoring the particle size and zeta potential of DMAS showed no significant changes in ultrapure water at room temperature (Supplementary Figure S3), demonstrating good long-term stability. These findings support the potential of using MPDA nanodrugs in various medical applications.

Drug Loading Ability of MPDA Nanodrugs

The drug loading capacity, encapsulation efficiency, and siRNA delivery efficiency of MPDA nanodrugs were evaluated. In our work, the drug loading capacity of DEX was approximately 36.04 ± 3.60%. The encapsulation efficiency of DEX in MPDA was approximately 72.63 ± 2.27% (Supplementary Figure S4). Previous studies have shown that non-porous PDA typically has a lower loading capacity of around 7 to 10%.[51,52] For the loading of VEGF-siRNA, the agarose gel electrophoresis results showed that when the DEX@MPDA-Arg (DMA) concentration reached 0.8 mg/mL, the siRNA band was nearly undetectable, suggesting complete encapsulation of siRNA (Supplementary Figure S5). Therefore, the concentration of 0.8 mg/mL was used for the synthesis of MPDA nanodrugs.

In Vitro Studies of MPDA Nanodrugs

In vitro studies of MPDA nanodrugs were conducted on HUVEC and RAW264.7 cells. As depicted in Figure 2A, DMAS had a negligible effect on cellular morphology at concentrations ranging from 0 to 50 μg/mL. This suggests that DMAS is well-tolerated by the cells within this concentration range. However, a decline in cell viability was observed when the concentration of DMAS went beyond 50 μg/mL. At concentrations between 0 and 50 μg/mL, HUVEC and RAW264.7 cells exhibited a high survival rate over 85% after 24 hours of incubation with various concentrations of MPDA nanodrugs (Supplementary Figure S6). This survival rate is well above the cytotoxicity threshold of 70%, as defined by ISO 10993–5.[53]

Subsequently, the ROS scavenging capability of DMAS was evaluated using a H_2O_2-induced oxidative stress model in RAW264.7 cells. The results showed that DMAS significantly reduced the intracellular ROS levels in H_2O_2-treated RAW264.7 cells compared to the MPDA-Arg (MA) group (Figure 2B and C). Notably, doping DEX with MPDA NPs demonstrated a significantly enhanced capability, as DEX is known for its ability to scavenge ROS.[54] DMAS showed a similar scavenging ability to DMA, suggesting that the addition of VEGF-siRNA did not enhance the ROS-scavenging ability.

The LPS-induced cell model was then used to test the anti-apoptotic ability and the anti-inflammatory effects of MPDA nanodrugs on HUVEC and RAW264.7 cells. Flow cytometry analysis (Figure 3A–D) revealed that LPS significantly increased the proportion of apoptotic cells compared to the PBS group, while DMAS significantly reduced apoptosis in LPS-treated cells. This indicates that DMAS possesses strong anti-apoptotic properties, which are particularly beneficial in inflammatory diseases where excessive apoptosis exacerbates tissue damage and disease progression.[55]

The effects of MPDA nanodrugs on inflammatory cytokine expression—including TNF-α, IL-6, IL-1β, and VEGF—were assessed in the LPS-induced cells. As shown in Figure 3E–G, MPDA nanodrugs significantly reduced the expression levels of IL-1β and TNF-α in LPS-induced RAW264.7 cells compared to the PBS control group. Notably, the DMAS group exhibited the lowest levels of IL-1β and IL-6 among the MPDA groups. Additionally, in LPS-induced HUVEC cells, DMAS reduced VEGF expression more effectively than DMA did (Figure 3H), underscoring its potential

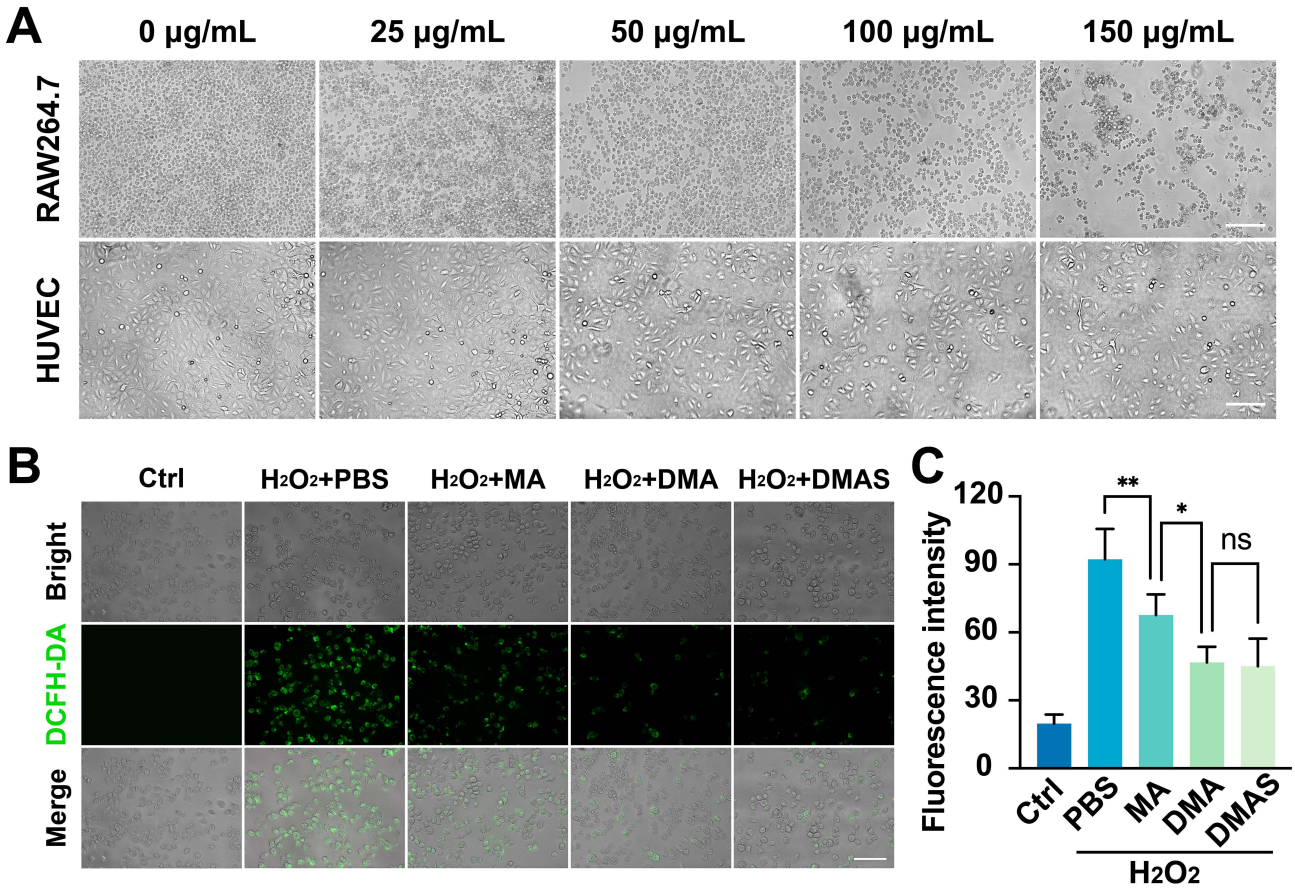

Figure 2 Biological effects of MPDA nanodrugs at cellular level. (**A**) Effects of different concentrations of DMAS on cell morphology. Scale bar: 200 μm. (**B**) Fluorescent images of intracellular ROS levels induced by H_2O_2 with MPDA nanodrugs. Scale bar: 100 μm. (**C**) Quantitative results of immunofluorescence intensity (n=5). The data are presented as mean ± SD with * indicating $P < 0.05$, ** indicating $P < 0.01$, and ns indicating no significant difference. Ctrl represents the blank control group.

in treating angiogenesis-driven diseases, such as cancer and DR. Overall, DMAS was the most effective in reducing inflammation-related cytokine levels compared to other MPDA nanodrugs.

Regarding the internalization and intracellular localization of the MPDA nanodrugs, the cellular uptake experiment demonstrated that the intracellular fluorescent signals from the fluorescein isothiocyanate (FITC)-DMAS were clearly tracked in HUVEC and RAW264.7 cells after 6 hours of incubation (Figure 3I). These results indicated that FITC-DMAS can effectively enter and accumulate within HUVEC and RAW264.7 cells.

In Vivo Studies with MPDA Nanodrugs

To validate the therapeutic efficacy of the MPDA nanodrugs, we employed three classic animal models (CoNV, OIR, and CNV mouse models) targeting different ocular segments—cornea, choroid, and retina—encompassing most types of ONDs, and simulating the pathological features of corneal alkali burn, ROP, and nAMD, respectively (Figure 4). To the best of our knowledge, this was the first study using PDA co-loaded with DEX and VEGF-siRNA on these OND animal models.

Therapeutic Effects of MPDA Nanodrugs in CoNV Mouse Model

The CoNV mouse model was established following a classical method (Supplementary Figure S7). To evaluate the local ocular biocompatibility of MPDA nanodrugs, Balb/c mice received subconjunctival injections of 5 μL MPDA nanodrugs at a concentration of 1 mg/mL, targeting the anterior segment of the eye. Slit lamp photography showed no signs of ocular redness, irritation, or inflammation at both 4-hour and 4-day time points (Supplementary Figure S8) after

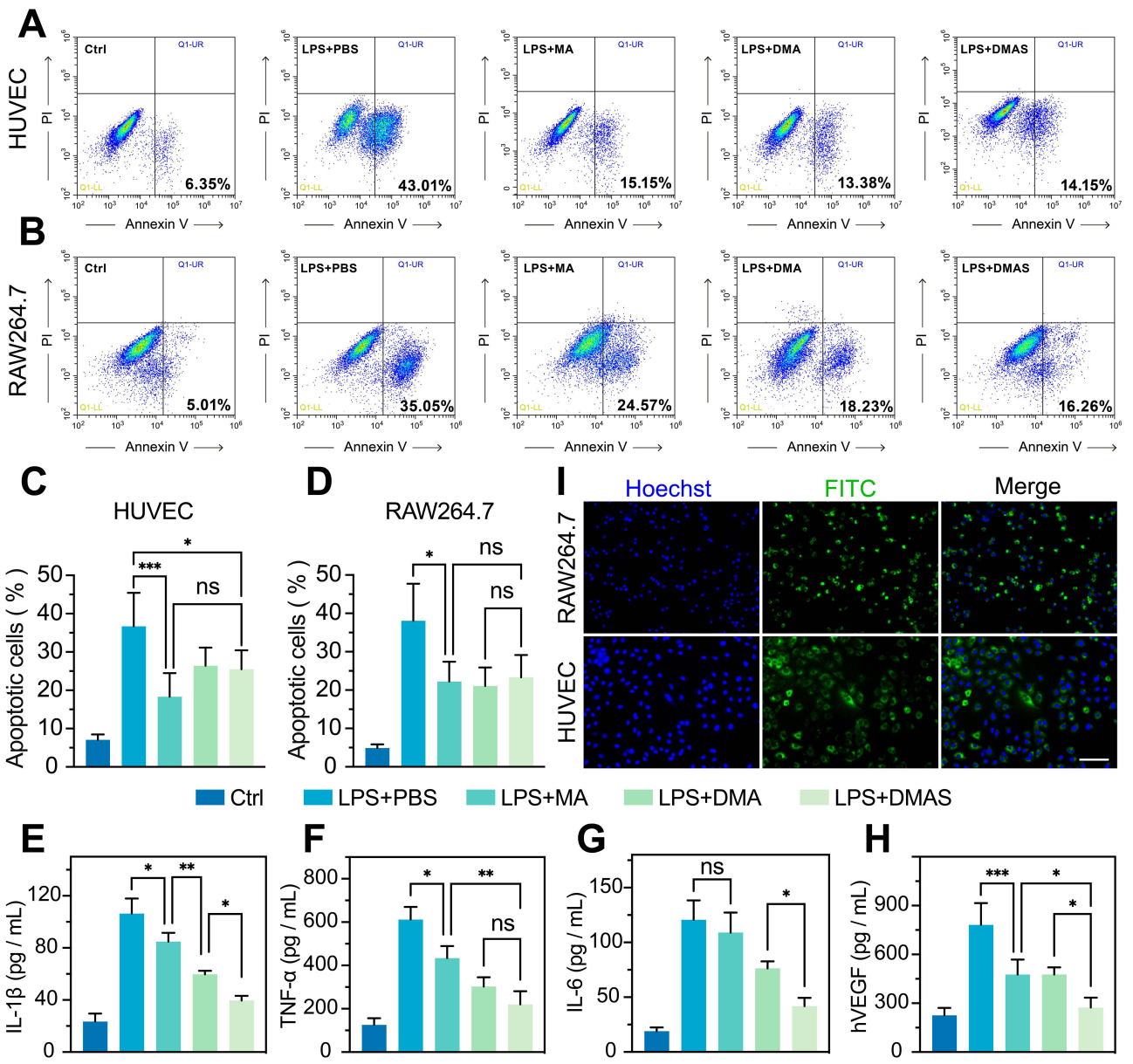

Figure 3 Anti-inflammatory and anti-apoptotic effects of MPDA nanodrugs at cellular level. (**A** and **B**) Effects of MPDA nanodrugs on apoptosis in HUVEC (**A**) and RAW264.7 (**B**) cells. (**C** and **D**) Percentage of apoptotic HUVEC (**C**) and RAW264.7 (**D**) cells induced by LPS (n=4). (**E-G**) Expression levels of IL-1β (**E**), TNF-α (**F**), and IL-6 (**G**) in the supernatant of RAW264.7 cells (n=3). (**H**) Expression levels of VEGF (n=4) in the supernatant of HUVEC cells. (**I**) Fluorescence microscopy observation of FITC-DMAS uptake. Scale bar: 100 μm. The data are presented as mean ± SD with * indicating $P < 0.05$, ** indicating $P < 0.01$, *** indicating $P < 0.001$, and ns indicating no significant difference. Ctrl represents the blank control group.

subconjunctival injection. This demonstrated the safety of the MPDA nanodrugs for ocular applications, particularly for the anterior segment of the eye. Thus, this concentration was used for further CoNV model studies.

The therapeutic effects of MPDA nanodrugs on the CoNV model were evaluated from four perspectives: CoNV inhibition, corneal repair, inflammation modulation, and corneal morphology. In terms of CoNV inhibition (Figure 5A), during the first two days post-alkali burn, neovascularization originated from the corneal margin and gradually extended towards the corneal center. The severity of CoNV was evaluated by measuring the CoNV length (Figure 5B) and scoring it (Figure 5C) on days 4, 7, 10, and 15. By day 10, all MPDA nanodrug treatments reduced neovascularization compared to PBS, with DMAS showing the most significant reductions by day 15. Additionally, the corneal optical opacity (Supplementary Figure S1) remained consistent across all groups at each observation point (Figure 5D).

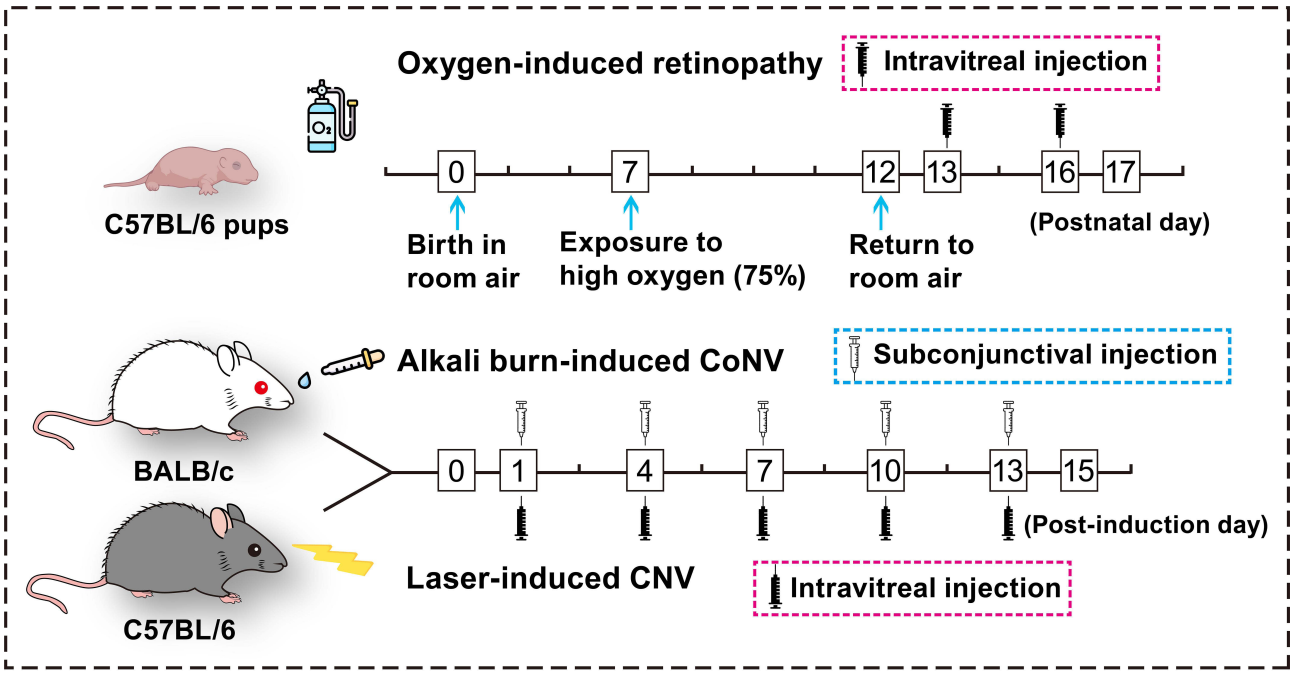

Figure 4 Experimental design of DMAS treatment on three OND animal models. The top timeline represents the OIR model in C57BL/6 pups, which involves exposure to 75% oxygen from postnatal day 7 to 12, then returning to room air, with intravitreal injections administered on postnatal days 13 and 16. The bottom timeline depicts the CoNV model in BALB/c mice, and laser-induced CNV model in C57BL/6 mice with intravitreal injections given on days 1, 4, 7, 10, and 13 post-induction.

Corneal epithelial defects, which served as an indicator of corneal repair, were noticeable in all groups one day post-alkali burn, as shown by fluorescein staining (Figure 5E). By day 4, DMAS significantly enhanced the healing rate of the corneal epithelium compared to PBS (Figure 5F), suggesting its ability to preserve the epithelial barrier and tight junctions, which are essential in preventing further damage and infection. By day 7, corneal epithelial defects were fully healed across all groups.

To assess corneal morphology, anterior segment-optical coherence tomography (AS-OCT) imaging was conducted in live mice (Figure 6A). AS-OCT analysis showed increased corneal thickness across all groups on day 1 post-alkali burn, with no significant thickness differences observed among groups, confirming consistent burn severity. High-density AS-OCT reflective signals in the anterior chamber suggested inflammatory exudates. By day 15, corneal thickness in the DMAS group was significantly lower than in the PBS, MA, DMA, and DEX groups (Figure 6B). Corneal thickness serves as a key indicator of corneal edema and tissue damage severity. Notably, anterior chamber depth remained consistent across treatments at any time point (Figure 6C), indicating that DMAS treatment likely targets the intended therapeutic areas without compromising the overall integrity of the anterior chamber.

To investigate the effects of different MPDA nanodrugs on corneal inflammation, we conducted flow cytometry to analyze CD31 and F4/80 expression in corneal tissue. CD31 is a critical marker for endothelial cells involved in angiogenesis and leukocyte migration,[56] and F4/80 is an essential marker for mature macrophages in CoNV formation.[57] Flow cytometry analysis (Supplementary Figures S9 and S10) revealed a notable reduction in CD31-positive cells within the DMAS group compared to the PBS group (Figure 6D). Additionally, F4/80-positive cells were reduced by approximately 37% in the DMAS group relative to the PBS group. Compared to DMAS, the DEX group showed a further reduction of around 50% in F4/80-positive cells (Figure 6E). These findings suggested that DMAS effectively suppressed both endothelial cell activation and macrophage infiltration, indicating its potential in reducing inflammatory responses associated with corneal neovascularization.

Histological examination using hematoxylin and eosin (H&E) staining (Figure 6F) revealed that DMAS-treated eyes showed reduced alkali-induced inflammatory cell infiltration, less disorganization of the corneal stroma, and better preservation of corneal structure compared to the PBS group. Additionally, among the MPDA nanodrug groups, the

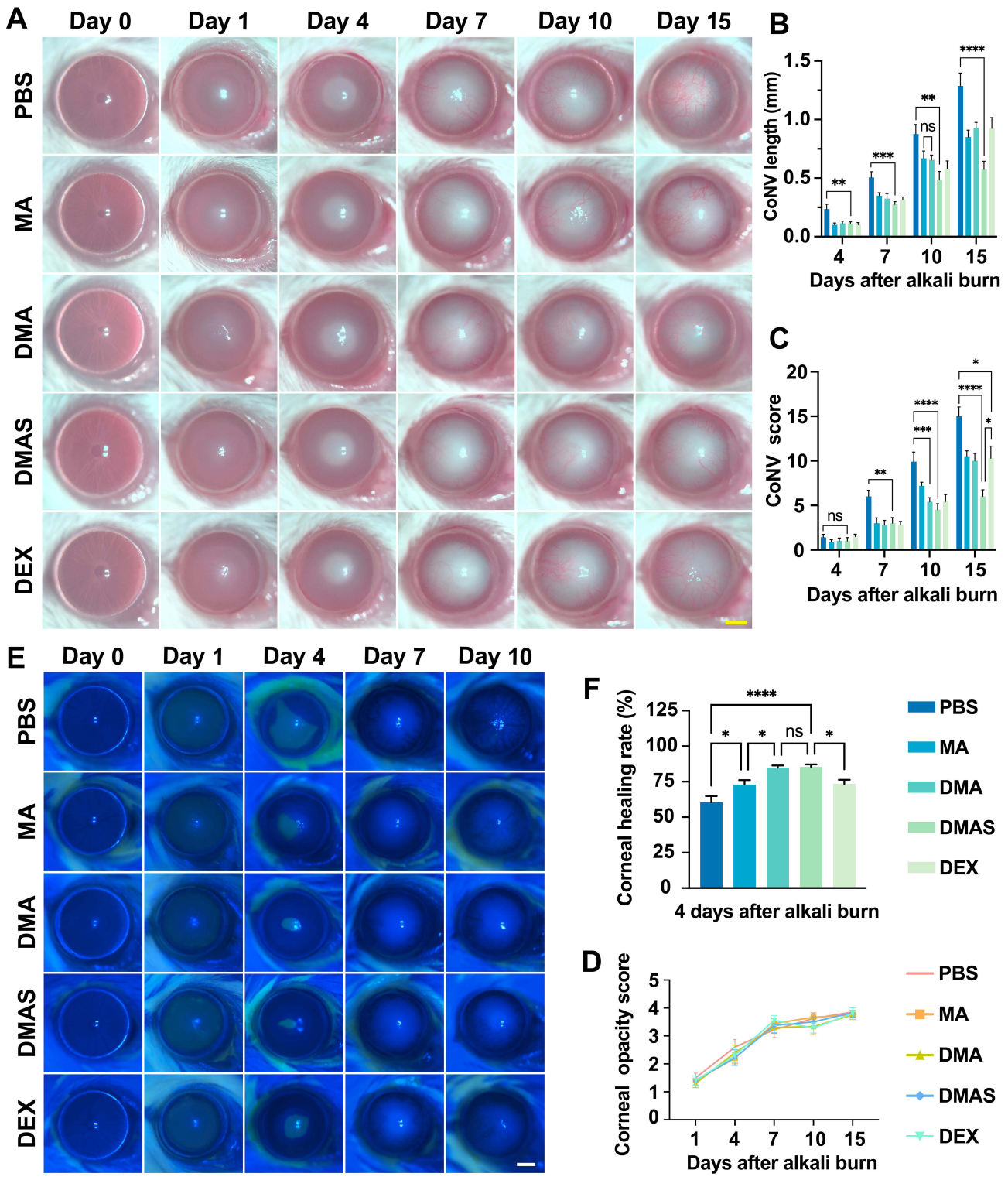

Figure 5 Therapeutic effects of MPDA nanodrugs on anti-angiogenic effects in CoNV model. (**A**) Slit-lamp observation of therapeutic effects of MPDA nanodrugs on CoNV in mice after alkali burn. Scale bar: 1 mm. (**B** and **C**) Quantification of CoNV length (**B**) and score (**C**) after alkali burn. (**D**) Progressive worsening of corneal optical opacity in all groups of mice after alkali burn. (**E**) Fluorescein sodium staining of corneal epithelial defects after alkali burn. Scale bar: 1 mm. (**F**) Quantification of the corneal epithelial defect healing rate on day 4 after alkali burn (n=7). The data are presented as mean ± SEM with * indicating $P < 0.05$, ** indicating $P < 0.01$, *** indicating $P < 0.001$, **** indicating $P < 0.0001$, and ns indicating no significant difference. Day 0 represents the stage without CoNV model establishment.

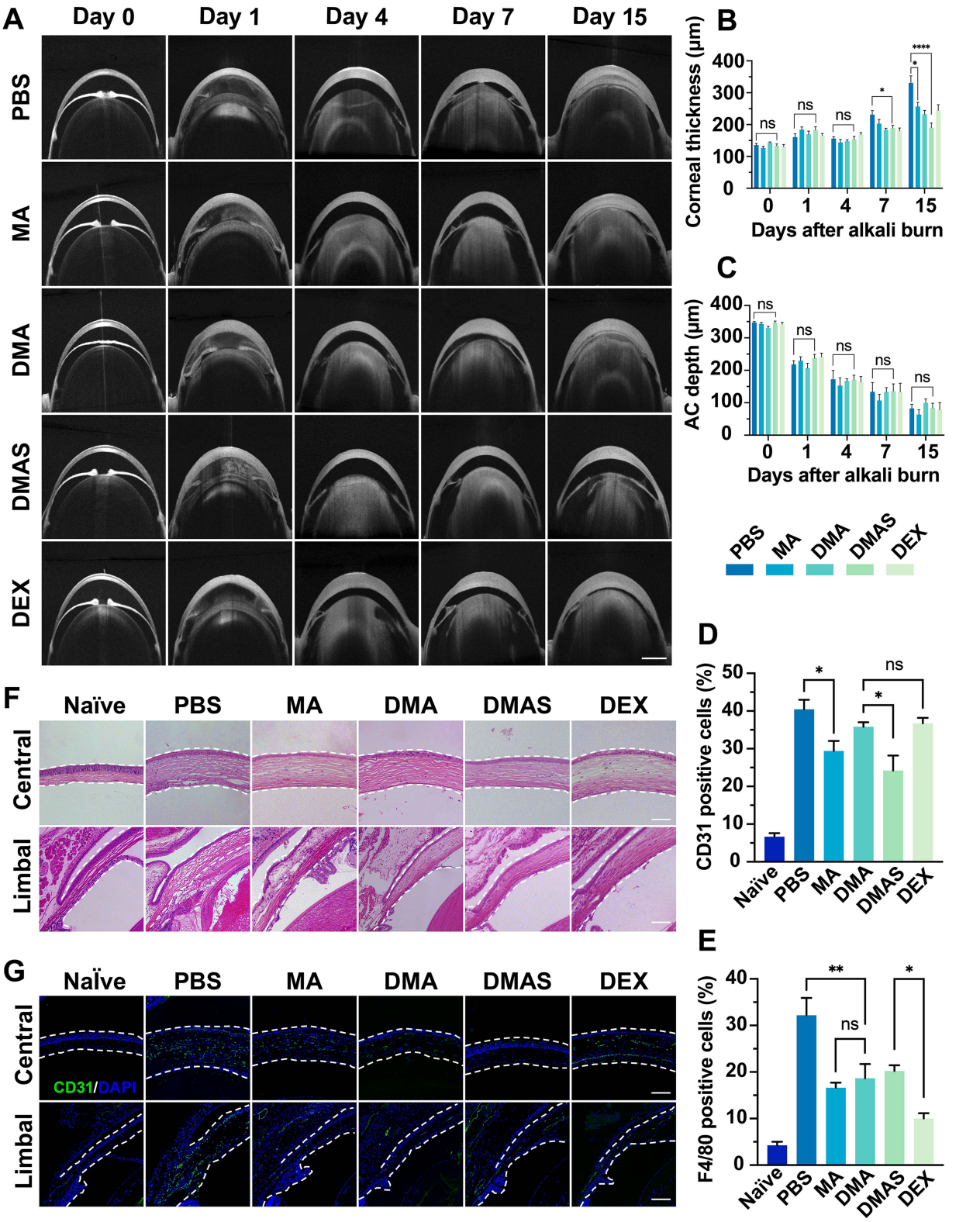

Figure 6 Therapeutic impact of DMAS nanodrugs on corneal inflammation and structural integrity in CoNV model. (**A**) AS-OCT results of anterior segment morphological changes in mice after alkali burn in different treatment groups. Scale bar: 500 μm. (**B** and **C**) Quantification of corneal thickness (**B**) and anterior chamber (AC) depth (**C**) in each group. (**D** and **E**) Percentage of CD31-positive (**D**) and F4/80-positive (**E**) cells in the conjunctival tissue of mice (n=4) on day 15 after alkali burn. (**F**) Histopathological features of the central (top panel) and limbal (bottom panel) structures of the cornea on day 15 after alkali burn. (**G**) Immunofluorescent staining of paraffin-embedded sections for CD31 expression on day 15 after alkali burn. The data are presented as mean ± SEM with *indicating $P < 0.05$, **indicating $P < 0.01$, ****indicating $P < 0.0001$, and ns indicating no significant difference. The white dashed line outlines the structure of the cornea. Naïve refers to mice not subjected to the alkali burn-induced CoNV model. Day 0 represents the stage without CoNV model establishment.

corneal histology in the DMAS group most closely resembled that of normal eyes. Immunofluorescent staining for CD31 (Figure 6G) aligned with flow cytometry findings, further verifying the effect of DMAS in lowering angiogenesis-related markers in the cornea. Furthermore, a comprehensive safety assessment, including hematological tests and histopathological analysis (Supplementary Figure S11), confirmed the ocular biocompatibility of MPDA nanodrugs (details available in Supplementary Materials).

Similar to the outcomes of our previous in vitro studies, the in vivo studies with DMAS treatment demonstrated the best performance in promoting corneal repair, modulating inflammation, and inhibiting CoNV, as compared to other single or dual-component treatments. Moreover, these findings further validate that the combination therapy of bioactive MPDA, anti-VEGF agents, and glucocorticoids like DEX offers synergistic benefits for addressing ONDs. Given the favorable results of DMAS in the CoNV model, we extended our research to two additional animal models: the OIR model and the laser-induced CNV model.

Therapeutic Effects of MPDA Nanodrugs in OIR Mouse Model

The OIR mouse model was established following a classical method (Supplementary Figure S12). To determine the anti-angiogenesis effect of MPDA nanodrugs, C57BL/6J suckling mice received intravitreal injections of 1 μL MPDA nanodrugs (1 mg/mL), targeting the posterior segment of the eye. On postnatal day 17, retinal vessels were stained with IB4 to visualize non-perfused areas and neovascularization. The results revealed a significant decrease in both retinal neovascularization and avascular area in the DMAS group compared to the other groups (Figure 7A–C).

Regarding the effects of MPDA nanodrugs on VEGF expression in the OIR retina, treatment with the MA groups (without loading VEGF-siRNA and DEX) showed a decreased level of VEGF in mouse retinal homogenates as compared to PBS groups (Figure 7D). More importantly, the DMAS group showed a significantly lower level of VEGF expression compared with other MPDA nanodrug groups, revealing a synergistic effect of combining VEGF-siRNA and DEX.

To further assess the effects of DMAS on blood vessels during sprouting angiogenesis, we analyzed serial sections of whole eyes from postnatal 17th day mice. H&E staining revealed endothelial cell nuclei on the surface of the retinal inner limiting membrane, with neovascular profiles extending into the vitreous cavity (Figure 7E). Compared to the PBS group, the DMAS group had notably fewer endothelial cell nuclei protruding through the retinal inner limiting membrane (Figure 7F), indicating that DMAS effectively inhibited new blood vessel growth from the retinal surface into the vitreous. Additionally, retinal thickness and morphology remained consistent across all OIR groups, suggesting that DMAS treatment did not compromise retinal structure, underscoring its biocompatibility with mouse retina (Supplementary Figure S13). See Supplementary Materials for more details.

Therapeutic Effects of MPDA Nanodrugs in CNV Mouse Model

The CNV mouse model was established in C57BL/6J mice using a classic method involving photocoagulation with a 532 nm laser, replicating the pathological features of nAMD.[58] Following laser injury, CNV lesions extended from the RPE layer into the retina. Fluorescein fundus angiography confirmed successful CNV induction by showing fluorescein leakage at lesion sites (Figure 8A). OCT angiography further revealed densely distributed CNV exhibiting a dendritic pattern within the laser spot area (Figure 8B). After the establishment of the CNV model, C57BL/6J mice received intravitreal injections of 1.5 μL MPDA nanodrugs at a concentration of 1 mg/mL, targeting the posterior segment of the eye.

To investigate the in vivo anti-angiogenic effect of the DMAS on the CNV model, the thickness of CNV lesions was measured using OCT (Figure 8C), while the CNV lesion areas were evaluated through immunofluorescent staining with IB4 (Figure 8D). By the 15th day post-laser injury, treatment groups (MA, DMA, DMAS, and DEX) significantly reduced CNV thickness compared to the control group (PBS, ~150 μm), with DMAS showing the most pronounced reduction (Figure 8E). Additionally, the DMAS group exhibited the smallest area of CNV lesions (Figure 8F), highlighting its superior therapeutic efficacy in ONDs. Furthermore, the intravitreal injection of all MPDA nanodrugs demonstrated good choroidal biocompatibility (Supplementary Figure S14), as described in the Supplementary Materials.

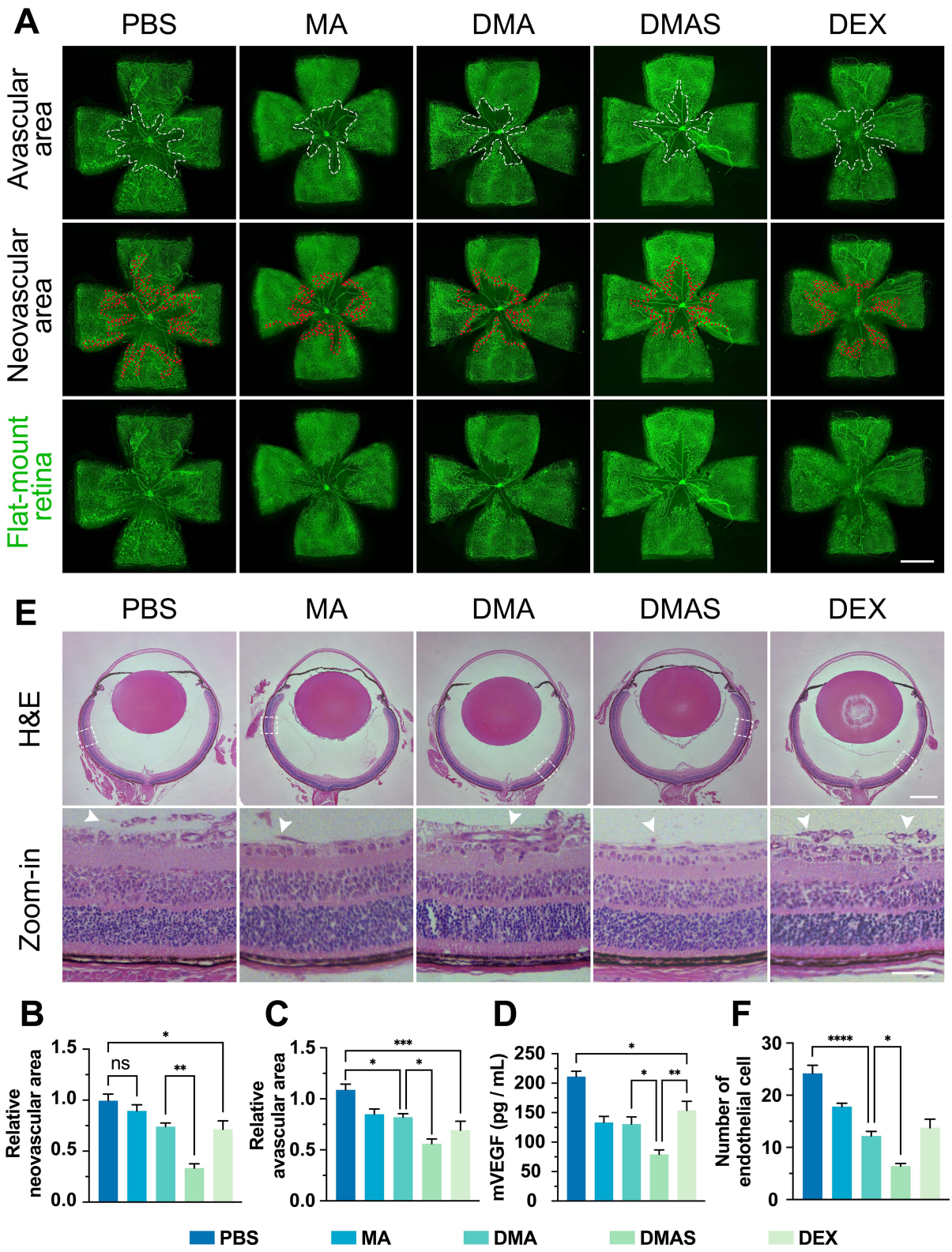

Figure 7 Anti-angiogenic effects of DMAS in OIR model. (**A**) IB4-stained retinal whole-mount images of C57BL/6J mice at postnatal 17th day. White dashed lines outline non-perfused regions, and red dots indicate neovascularization. Scale bar: 1 mm. (**B** and **C**) The relative area of retinal neovascularization (**B**) and non-perfused zone (**C**) in OIR mice. (**D**) Effects of MPDA nanodrugs on VEGF expression in retinal homogenates of mice (n=4). (**E**) H&E staining results of endothelial cell nuclei breaking through the retinal inner limiting membrane. The white arrows indicate the locations of the endothelial cell nuclei. In the H&E images, a scale bar of 1 mm is used for the general view, while a scale bar of 100 μm is applied for the zoom-in view. (**F**) Quantification of the number of endothelial cell nuclei breaking through the retinal inner limiting membrane. The data are presented as mean ± SEM with * indicating $P < 0.05$, **indicating $P < 0.01$, ***indicating $P < 0.001$, ****indicating $P < 0.0001$, and ns indicating no significant difference.

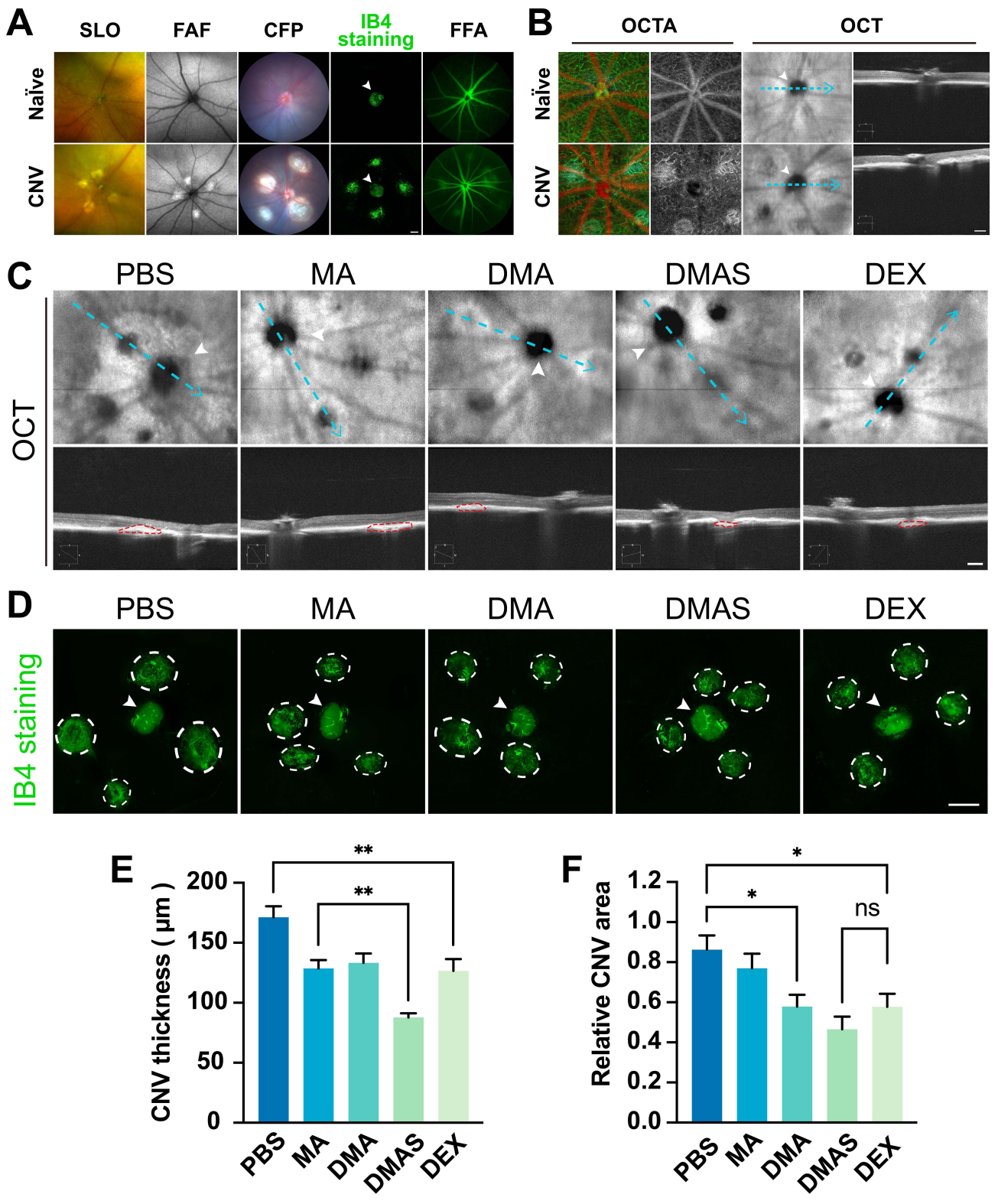

Figure 8 Anti-angiogenic effects of DMAS in laser-induced CNV model. (**A**) Comparison of fundus images before and after laser-induced CNV modeling using scanning laser ophthalmoscopy (SLO), fundus autofluorescence (FAF), color fundus photography (CFP), IB4 staining, and fundus fluorescein angiography (FFA). White arrows indicate the locations of the optic disc. Scale bar: 100 μm. (**B**) Optical coherence tomography angiography (OCTA) images demonstrate the morphological characteristics of CNV, with white arrows indicating the optic disc and blue dashed lines representing the OCT scanning lines. Scale bar: 200 μm. (**C**) Observation of CNV lesion thickness in mice using OCT, with blue dashed lines representing OCT scanning lines, white arrows denoting the optic disc, and red dashed lines indicating CNV lesions. Scale bar: 200 μm. (**D**) Immunofluorescence staining with IB4 was used to assess the CNV area, with white arrows indicating the locations of the optic disc. The area outlined by the dashed white circular line indicates the CNV region. Scale bar: 200 μm. (**E** and **F**) Quantitative OCT results of laser-induced CNV lesion thickness (**E**) and area (**F**) in mice. The data are presented as mean ± SEM with *indicating $P < 0.05$, **indicating $P < 0.01$, and ns indicating no significant difference. Naïve refers to mice not subjected to the laser-induced CNV model.

Biocompatibility of MPDA Nanodrugs

Slit lamp microscopy examination in mice without alkali burn revealed nearly no changes in the eye at 4 hours and 4 days post-subconjunctival injection of MPDA nanodrugs (Supplementary Figure S8). To further assess the potential systemic toxicity of MPDA nanodrugs, we performed the hematologic analyses in mice, and no abnormalities were observed in any parameters in comparison with the PBS-treated group (Supplementary Figures S11A-C and S14A-C). H&E staining also revealed no noticeable pathological abnormalities in the eyes (including eyeball, cornea, and retina) (Figures 6F and 7E) and major organs (including heart, liver, spleen, lung, and kidney) (Supplementary Figures S11E and S14D) of mice treated with MPDA nanodrugs. These findings collectively demonstrate that DMAS is a safe formulation, showing great promise for further application in inhibiting ocular neovascularization.

Discussion

Herein, we took advantage of the drug delivery capacity of polydopamine by developing the DMAS, an integrated nanodrug delivery system co-loaded with DEX and VEGF-siRNA for targeted anti-inflammatory and anti-angiogenic effects in ocular therapy. The DMAS nanoparticles exhibited favorable physicochemical properties, excellent cellular compatibility, and no observed ocular toxicity in vivo. Notably, in vitro experiments and trials across three animal models of ONDs confirmed the therapeutic efficacy of DMAS, showing significant anti-inflammatory, antioxidative, and angiogenesis inhibition effects, as well as enhanced corneal epithelial wound healing. These findings underscore that PDA-based DMAS is a safe, effective, and readily applicable nanodrug for topical OND treatment.

Adopting a synergistic therapy approach allows the encapsulation of multiple therapeutic agents within a single bioactive nanocarrier, optimizing the treatment process.[59] This method ensures simultaneous delivery of all components to the target site, enhancing their combined therapeutic potential while reducing systemic exposure and adverse effects. In our study, the DMAS nanodrug can simultaneously deliver VEGF-siRNA, a corticosteroid, and a bioactive PDA nanomaterial (Figure 1), each addressing different aspects of the treatment.[60] Specifically, VEGF-siRNA targets VEGF expression to inhibit neovascularization, beneficial in treating conditions such as nAMD and DR.[61] The corticosteroid provides robust anti-inflammatory effects, managing inflammation-related tissue damage and edema.[12] Meanwhile, PDA, with its antioxidant properties, scavenges ROS, reduces apoptosis, and protects ocular tissues.[62] Additionally, PDA stabilizes and enhances the effectiveness of the loaded drugs, enabling precise targeting and sustained therapeutic action.[63,64] Together, these components work synergistically to suppress pathological neovascularization, alleviate inflammation, reduce oxidative stress, and safeguard ocular tissues.

Our cell experiment results exhibited that the DMAS nanodrug showed the most potent synergistic effects, significantly reducing inflammatory cytokines (such as TNF-α, IL-6, and IL-1β) and VEGF expression (Figure 3E–3H) when compared to single or dual-component treatments. Various inflammatory mediators, including TNF-α and IL-6, have been associated with ONDs.[65] Additionally, VEGF plays a central role in vascular leakage and pathological neovascularization, with increased protein levels observed in conditions like nAMD, DR, diabetic macular edema, and ROP.[66] Thus, a therapeutic approach that combines anti-VEGF and anti-inflammatory strategies may provide enhanced benefits for ONDs. Our findings are consistent with previous studies,[67] which reported that integrating conbercept and MCC950 (an anti-inflammatory drug) into the hollow mesoporous silica nanoparticles significantly inhibited the expression of inflammatory factors (including intercellular adhesion molecule-1, monocyte chemoattractant protein 1, and IL-6) and VEGF at both mRNA and protein levels more effectively than single-component treatments. These findings further support the necessity of a collaborative therapeutic approach, including bioactive MPDA, targeted VEGF suppression, and anti-inflammatory effects, to enhance OND treatment outcomes.

Ocular injury can lead to CoNV, which can be effectively managed with anti-VEGF agents and corticosteroids.[68–70] Firstly, our study demonstrated that DMAS significantly inhibited corneal neovascularization, surpassing the efficacy of DEX (Figure 5A–C), a clinically used glucocorticoid known for its anti-angiogenic and anti-inflammatory properties.[71] Prior research has also shown that the combined use of DEX and bevacizumab in a CoNV rabbit model enhanced anti-angiogenic outcomes compared to monotherapy,[8] further aligning with our findings of a synergistic effect in CoNV inhibition using DMAS. Secondly, slit lamp photography showed no signs of ocular redness, irritation, or inflammation at both 4 hours and 4 days post-injection, demonstrating the baseline biocompatibility of the subconjunctival injection in healthy mice without alkali burn modeling. Thirdly, DMAS significantly accelerated corneal epithelial wound healing by day 4 post-alkali burn compared to the PBS group (Figure 5E and F). PDA promotes tissue repair through its antimicrobial and anti-inflammatory

properties, as well as by enhancing cell adhesion and proliferation.[72,73] Goswami et al found that DEX effectively aids corneal wound healing by reducing inflammation and preventing further damage from neovascularization.[15] Meanwhile, Fan et al demonstrated that PDA nanoparticles relieved inflammation and restored corneal structure in bacterial keratitis, exhibiting strong antibacterial effects.[74] Fourthly, a previous study demonstrated that anti-VEGF therapy effectively reduced CD31-marked CNV area and F4/80-positive macrophage percentages in a murine CNV model.[75] In our research, we observed comparable outcomes. Specifically, the DMAS nanodrug group showed significantly fewer CD31-positive and F4/80-positive cells in corneal and conjunctival tissues (Figure 6D and E), confirmed through immunohistochemical staining and flow cytometry. These results suggest that VEGF-siRNA, when combined with DEX, could outperform single-component treatments and may serve as a viable alternative to current anti-VEGF drugs in clinical applications.

Retinal neovascularization is characteristic of several pathological conditions, including DR and ROP, both of which can lead to vision loss.[76] Pathological angiogenesis in the retina is closely linked to inflammation, thereby contributing to the progression of ONDs.[77] Current treatments often require frequent intraocular injections of anti-VEGF drugs or the topical use of anti-inflammatory agents.[78] In our OIR mouse model, the DMAS nanodrug demonstrated the most significant reduction in retinal neovascularization, outperforming the DMA, MA, and DEX groups (Figure 7A–C). Additionally, VEGF levels were markedly lower in the DMAS group compared to other MPDA nanodrug groups (Figure 7D). This aligns with findings by Sardoiwala et al, where melanin-inspired PDA nanoparticles effectively reduced VEGF and ROS levels in the retinas of DR rats.[79] Moreover, clinical studies involving DEX and bevacizumab combination therapy have shown improvements in visual acuity and prolonged intervals between injections, reducing the treatment burden for patients and physicians alike.[80–82]

The development and progression of CNV are driven by pro-angiogenic factors, inflammatory proteins, and molecules impacting vascular permeability. Numerous studies, including both large-scale prospective and retrospective trials, have investigated the benefits of combining treatments for nAMD, using either sequential or simultaneous administration strategies.[81–83] Combination therapy, with separate administration of distinct drug components, has shown promise in treating CNV. For instance, one clinical study found that combining a DEX intravitreal implant with anti-VEGF agents led to a slight improvement in visual acuity in patients with treatment-resistant nAMD, as well as a reduction in the frequency of treatments required.[84] Similarly, Koss et al reported enhanced visual acuity with combined DEX and bevacizumab administration in CNV patients,[85] while Rezar-Dreindl et al observed improved outcomes with DEX implants plus ranibizumab compared to ranibizumab alone in recurrent CNV cases.[86] Our findings align with these studies, as the DMAS nanodrug significantly reduced both CNV thickness and area in the CNV mouse model, outperforming other single or dual-component treatments (Figure 8C–F).

Our study has certain limitations. While the DMAS nanomedicine showed anti-inflammatory, antioxidative, and anti- angiogenesis effects, the detailed molecular mechanisms remain to be fully elucidated. Advanced techniques, such as gene sequencing, transcriptomics, and proteomics, could be utilized in future research to reveal specific intracellular interactions. Additionally, we did not investigate a broad range of DMAS concentrations. Therefore, establishing a dose-response relationship would be valuable for optimizing therapeutic dosing. Lastly, although we focused on intravitreal and subconjunctival injections, exploring alternative delivery routes, such as eye drops and intracameral or subretinal injections, could potentially broaden the therapeutic application of DMAS.

Conclusions

In summary, we developed DMAS, a multifunctional nanodrug targeting various types of ONDs. Using three established animal models (CoNV, OIR, and CNV), we demonstrated that the combination of VEGF-siRNA, DEX, and bioactive MPDA showed complementary therapeutic effects, including anti-inflammatory, antioxidative, and anti-angiogenic properties, as well as promoting tissue repair. This study contributes to the field of ophthalmic nanomedicine, emphasizing the unique therapeutic benefits of PDA-based drug delivery systems for RNA and other drug compounds.

Acknowledgments

This work was financially supported by Shenzhen Science and Technology Program (No. JCYJ20210324113610029 and No. GJHZ20220913142618036).

Author Contributions

All authors made a significant contribution to the work reported, whether that is in the conception, study design, execution, acquisition of data, analysis and interpretation, or in all these areas; took part in drafting, revising or critically reviewing the article; gave final approval of the version to be published; have agreed on the journal to which the article has been submitted; and agree to be accountable for all aspects of the work.

Disclosure

The authors report no conflicts of interest in this work.

References

1. Carmeliet P, Jain RK. Molecular mechanisms and clinical applications of angiogenesis. *Nature*. 2011;473(7347):298–307. doi:10.1038/nature10144
2. Olsson AK, Dimberg A, Kreuger J, Claesson-Welsh L. VEGF receptor signalling - in control of vascular function. *Nat Rev Mol Cell Biol*. 2006;7(5):359–371. doi:10.1038/nrm1911
3. Sharma D, Zachary I, Jia H. Mechanisms of acquired resistance to anti-VEGF therapy for neovascular eye diseases. *Invest Ophthalmol Vis Sci*. 2023;64(5):28. doi:10.1167/iovs.64.5.28
4. Pauty J, Usuba R, Cheng IG, et al. A vascular endothelial growth factor-dependent sprouting angiogenesis assay based on an in vitro human blood vessel model for the study of anti-angiogenic drugs. *EBioMedicine*. 2018;27:225–236. doi:10.1016/j.ebiom.2017.12.014
5. Egwuagu CE, Sun L, Kim SH, Dambuza IM. Ocular inflammatory diseases: molecular pathogenesis and immunotherapy. *Curr Mol Med*. 2015;15(6):517–528. doi:10.2174/1566524015666150731095426
6. Daien V, Finger RP, Talks JS, et al. Evolution of treatment paradigms in neovascular age-related macular degeneration: a review of real-world evidence. *Br J Ophthalmol*. 2021;105(11):1475–1479. doi:10.1136/bjophthalmol-2020-317434
7. Tao T, Yang S, He D, et al. Intravitreal dexamethasone implants facilitate the management of refractory Behcet's uveitis with vasculitis. *Clin Immunol*. 2023;251:109633. doi:10.1016/j.clim.2023.109633
8. Kadar T, Amir A, Cohen L, et al. Anti-VEGF therapy (bevacizumab) for sulfur mustard-induced corneal neovascularization associated with delayed limbal stem cell deficiency in rabbits. *Curr Eye Res*. 2014;39(5):439–450. doi:10.3109/02713683.2013.850098
9. Perez-Gutierrez L, Ferrara N. Biology and therapeutic targeting of vascular endothelial growth factor A. *Nat Rev Mol Cell Biol*. 2023;24(11):816–834. doi:10.1038/s41580-023-00631-w
10. Hu W, Cai W, Wu Y, et al. Topical application of cell-penetrating peptide modified anti-VEGF drug alleviated choroidal neovascularization in mice. *Int J Nanomed*. 2024;19:35–51. doi:10.2147/IJN.S428684
11. Martens B, Drebert Z. Glucocorticoid-mediated effects on angiogenesis in solid tumors. *J Steroid Biochem Mol Biol*. 2019;188:147–155. doi:10.1016/j.jsbmb.2019.01.009
12. Gaballa SA, Kompella UB, Elgarhy O, et al. Corticosteroids in ophthalmology: drug delivery innovations, pharmacology, clinical applications, and future perspectives. *Drug Deliv Transl Res*. 2021;11(3):866–893. doi:10.1007/s13346-020-00843-z
13. Huang C, Zhang Z, Gu J, et al. Combined therapy of experimental autoimmune uveitis by a dual-drug nanocomposite formulation with berberine and dexamethasone. *Int J Nanomed*. 2023;18:4347–4363. doi:10.2147/IJN.S417750
14. Mishra N, Kant R, Kandhari K, et al. Establishing a dexamethasone treatment regimen to alleviate sulfur mustard-induced corneal injuries in a rabbit model. *J Pharmacol Exp Ther*. 2024;388(2):469–483. doi:10.1124/jpet.123.001680
15. Goswami DG, Mishra N, Kant R, et al. Effect of dexamethasone treatment at variable therapeutic windows in reversing nitrogen mustard-induced corneal injuries in rabbit ocular in vivo model. *Toxicol Appl Pharmacol*. 2022;437:115904. doi:10.1016/j.taap.2022.115904
16. Muns SM, Villegas VM, Flynn HW Jr, Schwartz SG. Update on current pharmacologic therapies for diabetic retinopathy. *Expert Opin Pharmacother*. 2023;24(14):1577–1593. doi:10.1080/14656566.2023.2230139
17. Amadio M, Govoni S, Pascale A. Targeting VEGF in eye neovascularization: what's new?: a comprehensive review on current therapies and oligonucleotide-based interventions under development. *Pharmacol Res*. 2016;103:253–269. doi:10.1016/j.phrs.2015.11.027
18. Alshaer W, Zureigat H, Al Karaki A, et al. siRNA: mechanism of action, challenges, and therapeutic approaches. *Eur J Pharmacol*. 2021;905:174178. doi:10.1016/j.ejphar.2021.174178
19. Zhang Y, Yuan Z, Jin Y, Zhang W, Yuan WE. Novel fluorinated spermine and small molecule PEI to deliver anti-PD-L1 and anti-VEGF siRNA for highly efficient tumor therapy. *Pharmaceutics*. 2021;13(12):2058. doi:10.3390/pharmaceutics13122058
20. Hu B, Zhong L, Weng Y, et al. Therapeutic siRNA: state of the art. *Signal Transduct Target Ther*. 2020;5(1):101. doi:10.1038/s41392-020-0207-x
21. Reghupaty SC, Sarkar D. Current status of gene therapy in hepatocellular carcinoma. *Cancers*. 2019;11(9):1265. doi:10.3390/cancers11091265
22. Singerman L. Combination therapy using the small interfering RNA bevasiranib. *Retina*. 2009;29:S49–50. doi:10.1097/IAE.0b013e3181ad2341
23. Kleinman ME, Yamada K, Takeda A, et al. Sequence- and target-independent angiogenesis suppression by siRNA via TLR3. *Nature*. 2008;452:591–597. doi:10.1038/nature06765
24. El Moukhtari SH, Garbayo E, Amundarain A, et al. Lipid nanoparticles for siRNA delivery in cancer treatment. *J Control Release*. 2023;361:130–146. doi:10.1016/j.jconrel.2023.07.054
25. Zhang MM, Bahal R, Rasmussen TP, Manautou JE, Zhong XB. The growth of siRNA-based therapeutics: updated clinical studies. *Biochem Pharmacol*. 2021;189:114432. doi:10.1016/j.bcp.2021.114432
26. Lyu Q, Hsueh N, Chai CLL. The chemistry of bioinspired catechol(amine)-based coatings. *ACS Biomater Sci Eng*. 2019;5(6):2708–2724. doi:10.1021/acsbiomaterials.9b00281
27. Lyu Q, Hsueh N, Chai CLL. Unravelling the polydopamine mystery: is the end in sight? *Polym Chem*. 2019;10(42):5771–5777. doi:10.1039/c9py01372e
28. Lyu Q, Zhang J, Neoh KG, Li Lin Chai C. A one step method for the functional and property modification of DOPA based nanocoatings. *Nanoscale*. 2017;9(34):12409–12415. doi:10.1039/c7nr05293f

29. Wu Y, Li X, Fu X, et al. Innovative nanotechnology in drug delivery systems for advanced treatment of posterior segment ocular diseases. *Adv Sci*. 2024;11:e2403399. doi:10.1002/advs.202403399
30. Friedrich M, Aigner A. Therapeutic siRNA: state-of-The-art and future perspectives. *BioDrugs*. 2022;36(5):549–571. doi:10.1007/s40259-022-00549-3
31. Wang J, Tao Z, Deng H, et al. Therapeutic implications of nanodrug and tissue engineering for retinal pigment epithelium-related diseases. *Nanoscale*. 2022;14(15):5657–5677. doi:10.1039/d1nr08337f
32. Yang W, Lyu Q, Zhao J, Cao L, Hao Y, Zhang H. Recent advance in near-infrared/ultrasound-sensitive 2D-nanomaterials for cancer therapeutics. *Sci China-Mat*. 2020;63(12):2397–2428. doi:10.1007/s40843-020-1387-7
33. Lyu Q, Peng L, Hong X, et al. Smart nano-micro platforms for ophthalmological applications: the state-of-The-art and future perspectives. *Biomaterials*. 2021;270:120682. doi:10.1016/j.biomaterials.2021.120682
34. Zhu M, Shi Y, Shan Y, et al. Recent developments in mesoporous polydopamine-derived nanoplatforms for cancer theranostics. *J Nanobiotechnol*. 2021;19(1):387. doi:10.1186/s12951-021-01131-9
35. Ma H, Peng J, Zhang J, et al. Frontiers in preparations and promising applications of mesoporous polydopamine for cancer diagnosis and treatment. *Pharmaceutics*. 2022;15(1):15. doi:10.3390/pharmaceutics15010015
36. Jin A, Wang Y, Lin K, Jiang L. Nanoparticles modified by polydopamine: working as ”drug” carriers. *Bioact Mater*. 2020;5(3):522–541. doi:10.1016/j.bioactmat.2020.04.003
37. Liu YC, Lin YK, Lin YT, et al. Injectable, antioxidative, and tissue-adhesive nanocomposite hydrogel as a potential treatment for inner retina injuries. *Adv Sci*. 2024;11(11):e2308635. doi:10.1002/advs.202308635
38. Zhang J, Jiao J, Niu M, et al. Ten years of knowledge of nano-carrier based drug delivery systems in ophthalmology: current evidence, challenges, and future prospective. *Int J Nanomed*. 2021;16:6497–6530. doi:10.2147/IJN.S329831
39. Gadde S. Multi-drug delivery nanocarriers for combination therapy. *MedChemComm*. 2015;6(11):1916–1929. doi:10.1039/C5MD00365B
40. Eftekhari RB, Maghsoudnia N, Samimi S, Zamzami A, Dorkoosh FA. Co-delivery nanosystems for cancer treatment: a review. *Pharm Nanotechnol*. 2019;7(2):90–112. doi:10.2174/2211738507666190321112237
41. Maturi RK, Bleau L, Saunders J, Mubasher M, Stewart MW. A 12-month, single-masked, randomized controlled study of eyes with persistent diabetic macular edema after multiple anti-VEGF injections to assess the efficacy of the dexamethasone-delayed delivery system as an adjunct to bevacizumab compared with continued bevacizumab monotherapy. *Retina*. 2015;35(8):1604–1614. doi:10.1097/IAE.0000000000000533
42. Fang Q, Liu S, Cui J, et al. Mesoporous polydopamine loaded pirfenidone target to fibroblast activation protein for pulmonary fibrosis therapy. *Front Bioeng Biotechnol*. 2022;10:920766. doi:10.3389/fbioe.2022.920766
43. Liu S, Zhang C, Zhou Y, et al. MRI-visible mesoporous polydopamine nanoparticles with enhanced antioxidant capacity for osteoarthritis therapy. *Biomaterials*. 2023;295:122030. doi:10.1016/j.biomaterials.2023.122030
44. Anderson C, Zhou Q, Wang S. An alkali-burn injury model of corneal neovascularization in the mouse. *J Vis Exp*. 2014;(86):51159. doi:10.3791/51159
45. Eaton JS, Miller PE, Bentley E, Thomasy SM, Murphy CJ. The SPOTS system: an ocular scoring system optimized for use in modern preclinical drug development and toxicology. *J Ocul Pharmacol Ther*. 2017;33(10):718–734. doi:10.1089/jop.2017.0108
46. Connor KM, Krah NM, Dennison RJ, et al. Quantification of oxygen-induced retinopathy in the mouse: a model of vessel loss, vessel regrowth and pathological angiogenesis. *Nat Protoc*. 2009;4(11):1565–1573. doi:10.1038/nprot.2009.187
47. Liu A, Liang C, Liu J, Huang Y, Wang M, Wang L. Reactive oxygen species horizontal line responsive lipid nanoparticles for effective RNAi and corneal neovascularization therapy. *ACS Appl Mater Interfaces*. 2022;14(15):17022–17031. doi:10.1021/acsami.1c23412
48. Cacua K, Ordonez F, Zapata C, Herrera B, Pabon E, Buitrago-Sierra R. Surfactant concentration and pH effects on the zeta potential values of alumina nanofluids to inspect stability. *Colloids Surfaces A*. 2019;583:123960. doi:10.1016/j.colsurfa.2019.123960
49. Chen T, Zhuang B, Huang Y, et al. Inhaled curcumin mesoporous polydopamine nanoparticles against radiation pneumonitis. *Acta Pharm Sin B*. 2022;12(5):2522–2532. doi:10.1016/j.apsb.2021.10.027
50. Hu H, Liu X, Hong J, et al. Mesoporous polydopamine-based multifunctional nanoparticles for enhanced cancer phototherapy. *J Colloid Interface Sci*. 2022;612:246–260. doi:10.1016/j.jcis.2021.12.172
51. Poinard B, Neo SZY, Yeo ELL, Heng HPS, Neoh KG, Kah JCY. Polydopamine nanoparticles enhance drug release for combined photodynamic and photothermal therapy. *ACS Appl Mater Interfaces*. 2018;10(25):21125–21136. doi:10.1021/acsami.8b04799
52. Wang Y, Huang Q, He X, et al. Multifunctional melanin-like nanoparticles for bone-targeted chemo-photothermal therapy of malignant bone tumors and osteolysis. *Biomaterials*. 2018;183:10–19. doi:10.1016/j.biomaterials.2018.08.033
53. Zaatreh S, Haffner D, Strauss M, et al. Fast corroding, thin magnesium coating displays antibacterial effects and low cytotoxicity. *Biofouling*. 2017;33(4):294–305. doi:10.1080/08927014.2017.1303832
54. Li Y, Liang Q, Zhou L, et al. An ROS-responsive artesunate prodrug nanosystem co-delivers dexamethasone for rheumatoid arthritis treatment through the HIF-1alpha/NF-kappaB cascade regulation of ROS scavenging and macrophage repolarization. *Acta Biomater*. 2022;152:406–424. doi:10.1016/j.actbio.2022.08.054
55. Bock FJ, Riley JS. When cell death goes wrong: inflammatory outcomes of failed apoptosis and mitotic cell death. *Cell Death Differ*. 2023;30(2):293–303. doi:10.1038/s41418-022-01082-0
56. Caligiuri G. CD31 as a therapeutic target in atherosclerosis. *Circ Res*. 2020;126(9):1178–1189. doi:10.1161/CIRCRESAHA.120.315935
57. Dos Anjos Cassado A. F4/80 as a major macrophage marker: the case of the peritoneum and spleen. *Results Probl Cell Differ*. 2017;62:161–179. doi:10.1007/978-3-319-54090-0_7
58. Wang Y, Liu CH, Ji T, et al. Intravenous treatment of choroidal neovascularization by photo-targeted nanoparticles. *Nat Commun*. 2019;10(1):804. doi:10.1038/s41467-019-08690-4
59. Jiang Y, Wang C, Zu C, Rong X, Yu Q, Jiang J. Synergistic potential of nanomedicine in prostate cancer immunotherapy: breakthroughs and prospects. *Int J Nanomed*. 2024;19:9459–9486. doi:10.2147/IJN.S466396
60. Lin D, Hu J, Wu K, et al. Synergistic effect of combined sub-tenon triamcinolone and intravitreal anti-VEGF therapy for uveitic macular edema. *Drug Des Devel Ther*. 2022;16:1055–1066. doi:10.2147/DDDT.S353251
61. Arrigo A, Aragona E, Bandello F. VEGF-targeting drugs for the treatment of retinal neovascularization in diabetic retinopathy. *Ann Med*. 2022;54(1):1089–1111. doi:10.1080/07853890.2022.2064541

62. Wu M, Hong C, Shen C, et al. Polydopamine nanomaterials and their potential applications in the treatment of autoimmune diseases. *Drug Deliv*. 2023;30(1):2289846. doi:10.1080/10717544.2023.2289846
63. Tang Y, Varyambath A, Ding Y, et al. Porous organic polymers for drug delivery: hierarchical pore structures, variable morphologies, and biological properties. *Biomater Sci*. 2022;10(19):5369–5390. doi:10.1039/d2bm00719c
64. Xiang S, Wang M, Li L, Shen J. Synergistic antibacterial effect of multifunctional TiO(2-X)-based nanoplatform loading arginine and polydopamine for promoting infected wounds healing. *Colloids Surf B Biointerfaces*. 2023;226:113332. doi:10.1016/j.colsurfb.2023.113332
65. Urias EA, Urias GA, Monickaraj F, McGuire P, Das A. Novel therapeutic targets in diabetic macular edema: beyond VEGF. *Vision Res*. 2017;139:221–227. doi:10.1016/j.visres.2017.06.015
66. Becker K, Weigelt CM, Fuchs H, et al. Transcriptome analysis of AAV-induced retinopathy models expressing human VEGF, TNF-alpha, and IL-6 in murine eyes. *Sci Rep*. 2022;12(1):19395. doi:10.1038/s41598-022-23065-4
67. Sun J, Nie H, Pan P, et al. Combined anti-angiogenic and anti-inflammatory nanoformulation for effective treatment of ocular vascular diseases. *Int J Nanomed*. 2023;18:437–453. doi:10.2147/IJN.S387428
68. Eiger-Moscovich M, Livny E, Sella R, et al. Comparison of subconjunctival aflibercept and betamethasone for the treatment of formed corneal neovascularization in a rabbit model. *Ophthalmic Res*. 2019;62(2):116–122. doi:10.1159/000499165
69. Zhang C, Yin Y, Zhao J, et al. An update on novel ocular nanosystems with possible benefits in the treatment of corneal neovascularization. *Int J Nanomed*. 2022;17:4911–4931. doi:10.2147/IJN.S375570
70. Gore A, Horwitz V, Cohen M, et al. Successful single treatment with ziv-aflibercept for existing corneal neovascularization following ocular chemical insult in the rabbit model. *Exp Eye Res*. 2018;171:183–191. doi:10.1016/j.exer.2018.03.010
71. Yin Q, Han H, Shi K, et al. Targeted dexamethasone nano-prodrug for corneal neovascularization management. *Biomed J*. 2024;47(1):100592. doi:10.1016/j.bj.2023.03.005
72. Zheng D, Huang C, Zhu X, Huang H, Xu C. Performance of polydopamine complex and mechanisms in wound healing. *Int J Mol Sci*. 2021;22(19):10563. doi:10.3390/ijms221910563
73. Kwon YS, Munsoor J, Kaufmann M, Zheng M, Smirnov AI, Han Z. Polydopamine nanoparticles as mimicking RPE melanin for the protection of retinal cells against blue light-induced phototoxicity. *Adv Sci*. 2024;11:e2400230. doi:10.1002/advs.202400230
74. Fan W, Han H, Lu Z, et al. Epsilon-poly-L-lysine-modified polydopamine nanoparticles for targeted photothermal therapy of drug-resistant bacterial keratitis. *Bioeng Transl Med*. 2023;8(1):e10380. doi:10.1002/btm2.10380
75. Lee SHS, Kim HJ, Shin OK, et al. Intravitreal injection of AAV expressing soluble VEGF receptor-1 variant induces anti-VEGF activity and suppresses choroidal neovascularization. *Invest Ophthalmol Vis Sci*. 2018;59(13):5398–5407. doi:10.1167/iovs.18-24926
76. Yu Y, Tomlinson LA, Binenbaum G, Ying GS, Group GRS. Incidence, timing and risk factors of type 1 retinopathy of prematurity in a North American cohort. *Br J Ophthalmol*. 2021;105(12):1724–1730. doi:10.1136/bjophthalmol-2020-317467
77. Tian Y, Zhang F, Qiu Y, et al. Reduction of choroidal neovascularization via cleavable VEGF antibodies conjugated to exosomes derived from regulatory T cells. *Nat Biomed Eng*. 2021;5(9):968–982. doi:10.1038/s41551-021-00764-3
78. Campochiaro PA. Molecular pathogenesis of retinal and choroidal vascular diseases. *Prog Retin Eye Res*. 2015;49:67–81. doi:10.1016/j.preteyeres.2015.06.002
79. Sardoiwala MN, Nagpal S, Bhatt B, Roy Choudhury S, Karmakar S. Improved melatonin delivery by a size-controlled polydopamine nanoformulation attenuates preclinical diabetic retinopathy. *Mol Pharm*. 2023;20(6):2899–2910. doi:10.1021/acs.molpharmaceut.2c01039
80. Limon U, Sezgin Akcay BI. Add-on effect of simultaneous intravitreal dexamethasone to intravitreal bevacizumab in patients with macular edema secondary to branch retinal vein occlusion. *J Ocul Pharmacol Ther*. 2022;38(2):183–188. doi:10.1089/jop.2021.0100
81. Englander M, Kaiser PK. Combination therapy for the treatment of neovascular age-related macular degeneration. *Curr Opin Ophthalmol*. 2013;24(3):233–238. doi:10.1097/ICU.0b013e32835f8eaa
82. Jonas JB, Libondi T, Golubkina L, Spandau UH, Schlichtenbrede F, Rensch F. Combined intravitreal bevacizumab and triamcinolone in exudative age-related macular degeneration. *Acta Ophthalmol*. 2010;88(6):630–634. doi:10.1111/j.1755-3768.2008.01502.x
83. Couch SM, Bakri SJ. Review of combination therapies for neovascular age-related macular degeneration. *Semin Ophthalmol*. 2011;26(3):114–120. doi:10.3109/08820538.2011.577130
84. Todorich B, Thanos A, Yonekawa Y, et al. Simultaneous dexamethasone intravitreal implant and anti-VEGF therapy for neovascular age-related macular degeneration resistant to anti-VEGF monotherapy. *J Vitreoretin Dis*. 2017;1(1):65–74. doi:10.1177/2474126416683299
85. Koss MJ, Scholtz S, Haeussler-Sinangin Y, Singh P, Koch FH. Combined intravitreal pharmacosurgery in patients with occult choroidal neovascularization secondary to wet age-related macular degeneration. *Ophthalmologica*. 2010;224(2):72–78. doi:10.1159/000235724
86. Rezar-Dreindl S, Eibenberger K, Buehl W, et al. Role of additional dexamethasone for the management of persistent or recurrent neovascular age-related macular degeneration under Ranibizumab treatment. *Retina*. 2017;37(5):962–970. doi:10.1097/IAE.0000000000001264